Polarization mode dispersion spectrum measurement via high-speed wavelength-parallel polarimetry

Li Xu,[1,*] Shawn X. Wang,[1,2] Houxun Miao,[1,3] and Andrew M. Weiner[1]

[1]Department of Electrical and Computer Engineering, Purdue University, West Lafayette, Indiana 47907-2035, USA

[2]Currently with the Department of Electrical Engineering, Northwestern University, Evanston, Illinois 20208, USA

[3]Currently with the Center for Nanoscale Science and Technology, National Institute of Standards and Technology, Gaithersburg, Maryland 20899-6203, USA

*Corresponding author: xu36@purdue.edu

Received 9 April 2009; revised 17 July 2009; accepted 24 July 2009; posted 28 July 2009 (Doc. ID 109790); published 11 August 2009

We report experiments in which wavelength-parallel spectral polarimetry technology is used for measurement of the frequency-dependent polarization mode dispersion (PMD) vector. Experiments have been performed using either a grating spectral disperser, configured to provide 13.6 GHz spectral resolution over a 14 nm optical bandwidth, or a virtually imaged phased array spectral disperser, configured for 1.6 GHz spectral resolution over a 200 GHz band. Our results indicate that the spectral polarimetry data obtained via this approach are of sufficient quality to permit accurate extraction of the PMD spectrum. The wavelength-parallel spectral polarimetry approach allows data acquisition within a few milliseconds. © 2009 Optical Society of America

OCIS codes: 060.2330, 060.2340, 060.2370, 260.5430.

1. Introduction

Polarization mode dispersion (PMD) [1] is a fundamental phenomenon that limits the bandwidth of high-speed optical fiber communication systems. PMD arises from the residual birefringence of the optical fiber and the random orientation of the birefringence axes, which cause a differential group delay (DGD) between orthogonal polarization modes. If the delay is comparable to a significant fraction of the bit period, adjacent bits may overlap to degrade system performance.

PMD is fully described by the frequency-dependent PMD vector, which specifies both the DGD spectrum and the principal state of polarization (PSP) spectrum [1]. Since the variation of PMD can occur occasionally on a millisecond scale [2], the capability of fast monitoring for PMD is desirable. Furthermore, since the frequency dependence of the PMD vector becomes important for large DGD [1,3], a frequency-resolved monitoring tool with sufficient spectral resolution may be preferred. Although it is possible to use commercial instrumentation for fast single channel polarization measurement, fast measurement of frequency-dependent polarization is still largely undeveloped. Our laboratory has recently developed a novel wavelength-parallel polarimeter [4,5], which provides unique capabilities for high-speed (millisecond time scale) characterization of frequency-dependent PMD. The wavelength-parallel polarimeter has been successfully applied to monitor frequency-dependent states of polarization (polarization string lengths) in a commercial 10 Gbit/s WDM optical transmission system [6]. This experiment demonstrated a tight correlation between the string length [7] and PMD-induced bit error rates, thereby providing evidence for polarization string length as an effective parameter for in-service PMD monitoring. Our wavelength-parallel polarimeter has also been employed successfully in experiments to demonstrate all-order PMD compensation [8,9]. In these experiments the polarimeter was used to

0003-6935/09/244688-10$15.00/0

acquire data (either the frequency-dependent state of polarization [8] or the frequency-dependent Jones matrix [9]) needed for control of the optical all-order PMD compensator.

In these previous reports, however, the frequency-dependent PMD vector itself was not obtained. Extracting the PMD vector requires the operation of taking frequency derivatives, which places much more stringent demands on the quality and accuracy of the polarimetry data. In this paper, for the first time to our knowledge, we demonstrate extraction of the frequency-dependent PMD vector using the wavelength-parallel polarimeter (a preliminary description of these experiments was reported in [10]). In order to confirm the accuracy of our results, we first perform measurements with simple PMD emulators for which characteristics of the frequency-dependent PMD vector can be calculated *a priori*. For more complicated emulators, we compare the results of two different algorithms for extracting the PMD vector from different sets of polarimetery data. Furthermore, we perform experiments with two different wavelength-parallel polarimeters, one with relatively wide optical bandwidth (14 nm) and coarse spectral resolution (13.6 GHz) and the second with narrower optical bandwidth (1.6 nm) but much finer spectral resolution (1.6 GHz). The latter setup allows measurements with very large PMD, up to 90 ps of mean DGD. In all cases the data appear to be of excellent quality.

The remainder of this paper is structured as follows. In Section 2 we discuss the setup and the experimental procedures. This section specializes to the case of the wide bandwidth, coarse resolution wavelength-parallel polarimeter, which is based on a diffraction grating spectral disperser. Experimental results are given in Section 3, with a focus on extracted frequency-dependent PMD vectors. In Section 4 we present experiments performed with the narrow bandwidth, high spectral resolution polarimeter, which is based on a virtually imaged phased array (VIPA) [11,12] as the spectral disperser. We conclude in Section 5.

2. Polarization Mode Dispersion Measurement Scheme

A. Experimental Setup

Our experimental setup is composed of a multiple states of polarization (multi-SOP) generator, a PMD emulator, and a spectral (wavelength-parallel) polarimeter, as shown in Fig. 1. The spectral polarimeter consists of an SOP components selector, a spectral disperser with a grating and lens, and a one-dimensional infrared camera. The multi-SOP generator and spectral polarimeter are both computer controlled. Data are acquired using an SCB-68 high-speed data acquisition board from National Instruments. An amplified spontaneous emission (ASE) light source (OPREL BBS-30-F2-141) was used in all our measurements. It provides broadband unpolarized light with 16 dBm power spanning much of the lightwave C band. In the experimental procedure, the light from the ASE source first passes through a multi-SOP generator capable of rapidly cycling through various desired input SOPs. The polarized light is then launched into a PMD emulator, which we also refer to as the device under test (DUT). Finally, a spectral polarimeter setup is placed at the output of the PMD emulator to capture the SOP spectra for the PMD vector calculations.

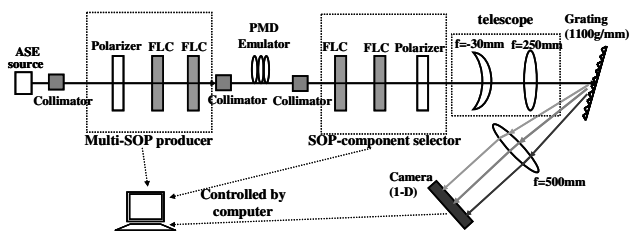

Fig. 1. PMD measurement setup with a grating as spectral disperser.

B. Ferroelectric Liquid Crystals for Multiple States of Polarization Generation and Polarimetry

In our multi-SOP generation and SOP measurement, the ferroelectric liquid crystal (FLC) cell is a key component providing high-speed polarization control. Figure 2 shows the function of an FLC cell, which works as a waveplate with rapidly switchable optical axes. The birefringence axis can be switched within 100 μs between two stable states separated by approximately 45° by applying opposite voltage polarities (±5 V). In our experiments all of the FLC cells are designed for quarter-wave retardance.

By placing a pair of these FLC cells after a polarizer, it is possible to generate up to four different SOPs. Our setup is designed to provide 0°, 90°, and 135° linear SOP as well as right-hand circular (RHC) SOP. To realize this, the polarizer is 0° oriented. The fast axis of the first FLC cell switches between 0° and 45°, and the second FLC cell 45° and 90°. The truth table for SOP generation is shown in Table 1. This SOP generation scheme meets different requirements for compatibility with different algorithms for PMD vector measurement. For example, for the Jones matrix eigenanalysis method (JME) [13], we generate 0°, 90°, and 135° linear SOPs. For the Müller matrix method (MMM) [14], we use 0° and RHC as input SOPs.

FLCs are also used in our spectral polarimeter [4,5] for SOP component selection. Here we place a

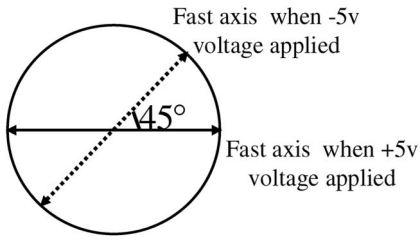

Fig. 2. FLC cell.

Table 1. Truth Table for Multi-SOP (State of Polarization) Generator

Polarizer	Fast Axis Direction: First $\lambda/4$ FLC	Fast Axis Direction: Second $\lambda/4$ FLC	SOP Generated
Fixed at 0°	45°	90°	135°
	45°	45°	90°
	0°	90°	0°
	0°	45°	RHC

fixed polarizer after two FLCs and switch the two FLCs to provide four distinct polarization transformations, as shown in Table 2. Thus we can sequentially measure the intensity of four different SOP components, I_0, I_{90}, I_{135}, and I_{RHC}, which fully determine the SOP.

C. Spectral Polarimetry

In addition to the FLC cells, the spectral polarimeter contains a diffraction grating (1100 grooves/mm) and an InGaAs line-scan camera (with each pixel 50 μm wide) as a detector array, as shown in Fig. 1. Our setup provides a frequency span of 1542.9 to 1556.9 nm across the 128 pixels of the camera, and a spectral resolution of 13.6 GHz/pixel. For a CW laser beam centered on one camera pixel, the signal detected on nearest neighbor pixels is suppressed by 3 dB. Assisted by the parallel detection, the measurement speed can be very fast. The camera itself can measure and read out all 128 pixels within ~50 μs. The switching time of the FLC cells can be as fast as 100 μs. One complete set of SOP measurements (performed in parallel for 128 wavelengths) requires cycling through four FLC states. Therefore the total time can be under 1 ms for data acquisition (followed by offline software processing). The data acquisition speed in the current experiment is limited to 20 ms by the software control. We have however demonstrated less than 1 ms data acquisition speed by using external timing circuits to control FLC and camera triggering. We use a calibration and correction procedure described in [4,5] to account for the frequency dependence of the FLCs. The resulting SOP error was observed to be less than 2° on the Poincaré sphere.

D. Polarization Mode Dispersion Emulator

Several homemade PMD emulators are used as our DUT. These homemade emulators are concatenations of various lengths of polarization-maintaining fibers (PMFs). Each PMF section can be viewed as a retarder, with refractive index difference $\Delta n \sim 4.15 \times 10^{-4}$ between the fast and slow axes. We use various numbers of PMF sections with fast axes offset by different angles to produce the desired PMD. Moreover, standard single-mode fibers (SMFs) are spliced at both ends as leads. For some of the simple (few sections) PMD emulators, we are able to calculate their PMD characteristics from their known construction parameters (fiber lengths and splice angles) and compare directly with measurement results. Theoretically, the PMD vectors of these emulators can be estimated using the PMD vector concatenation rule [1]. It states that for concatenation of two elements with output PMD vector $\vec{\tau}_1$ and $\vec{\tau}_2$, respectively, the total output PMD vector is

$$\vec{\tau}(\omega) = \vec{\tau}_2 + R_2(\omega)\vec{\tau}_1, \tag{1}$$

where $R_2(\omega)$ is the SOP rotation matrix (Müller matrix) of the second element. This equation can be applied repeatedly to obtain the total PMD vector of multiple concatenated PMD elements.

However, when we estimate the PMD of this kind of emulator, we have two difficulties. First, the output lead rotates the output PSPs on the Poincaré sphere in an unknown (but approximately frequency-independent) way. Second, our measurement of the lengths of PM fiber sections has error comparable to the fiber beat length of ~3 mm; this implies large error in estimating the SOP rotation matrix of a PMF section. As a result, it is not practical to calculate the exact PMD vector of these emulators. However, the following three special cases corresponding to few-section emulators do have certain parameters that can be accurately determined. We illustrate these by the simulation results in Fig. 3.

The first (simplest) case is that of one section of PMF. Both its DGD and PSP are frequency independent, corresponding to a fixed point on the Poincaré sphere as in Figs. 3(a) and 3(b). The DGD is estimated by

$$\Delta\tau = \Delta n \times L/c, \tag{2}$$

where L is the PMF length.

The second case is the concatenation of two PMF sections with lengths L_1 and L_2 and offset angle θ between the two fast axes. By the concatenation rule for the PMD vector, the DGD is

$$\Delta\tau = \sqrt{L_1^2 + L_2^2 + 2L_1L_2\cos 2\theta}\cdot \Delta n/c, \tag{3}$$

which is a frequency-independent constant. As for the PSP, we cannot calculate the exact value because of the rotation of the SMF lead at the output side and the inability to precisely know the SOP rotation matrix of the second PMF section. However, the PSP spectrum can be shown to follow a circular trajectory

Table 2. Truth Table for SOP (State of Polarization) Component Selector

Fast Axis Direction: First $\lambda/4$ FLC	Fast Axis Direction: Second $\lambda/4$ FLC Fast Axis Direction	Polarizer	SOP Selected
90°	0°	Fixed at 0°	0°
135°	135°		90°
90°	135°		45°
135°	0°		RHC

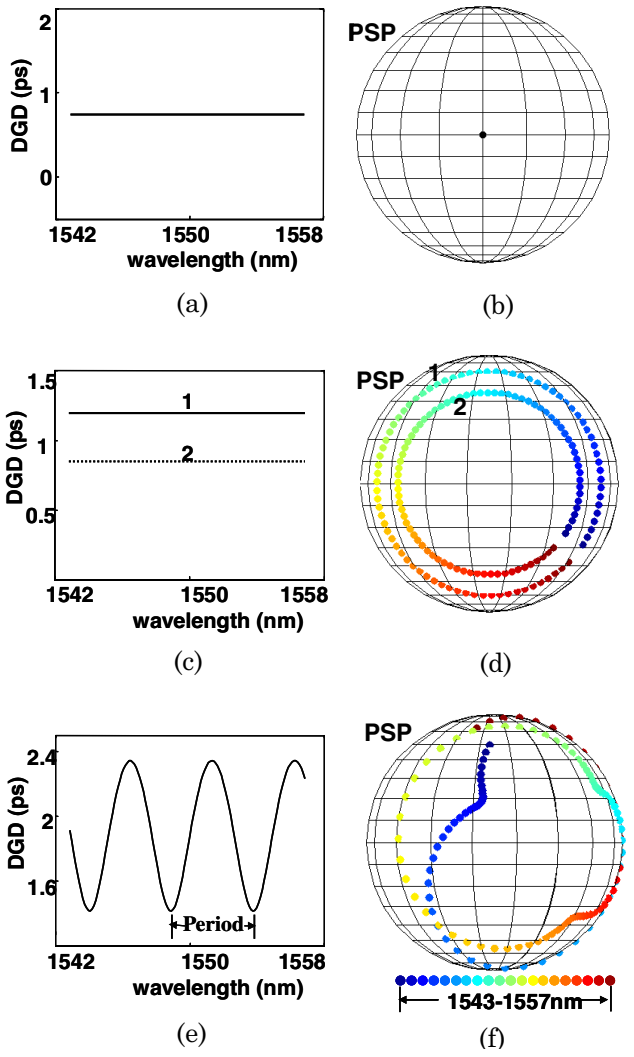

Fig. 3. (Color online) DGD and PSP by simulation: (a), (b) 1-section emulator; (c), (d) 2-section emulator, where we put two cases together. Case 1 stands for the 70 cm + 40 cm PMF concatenation with 45° fast axes offset. In case 2, the first PMF section is shortened from 70 to 40 cm to get 40 cm + 40 cm concatenation and the fast axis offset is left unchanged. (e), (f) 3-section emulator (59.2 cm + 118.5 cm + 83 cm, two fast axes offsets are both 45°).

on the Poincaré sphere with radius r determined by L_1/L_2 and θ:

$$r = \sin\left(\cos^{-1}\left(\frac{1 + L_1/L_2 \cdot \cos 2\theta}{\sqrt{1 + L_1^2/L_2^2 + 2L_1/L_2 \cdot \cos 2\theta}}\right)\right). \tag{4}$$

We cannot calculate the position on the PSP circle for any specific frequency. But if we cut the length L_1 of the first PMF section from the input side without touching the second PMF or the output side SMF lead, we expect the PSP circle to remain concentric with the original PSP circle. More specifically, PSPs for a fixed optical frequency retain a fixed angular location on the concentric PSP circles. Figures 3(c) and 3(d) show PMD simulation results for this second case.

The third case with calculable parameters is the concatenation of three sections of PMF. For the same reasons as above, the DGD and PSP for individual frequencies cannot be accurately calculated. However, the DGD spectrum can be shown to be periodic, as shown in Fig. 3(e). The period is determined by the length of the second PMF L_2 according to

$$\Delta\omega = 2\pi c/(\Delta n L_2). \tag{5}$$

The PSP trajectory, shown in Fig. 3(f), is more complicated than a circle, and it has no calculable parameters.

To perform estimation by Eqs. (2)–(5), we measured several parameters: fiber length L, birefringence Δn, and fast axis offset angle θ. As for fiber length L, each section has an error of ~1 mm. This is less than 0.2% of the lengths of the sections, which are all larger than 50 cm. In the measurement of birefringence Δn, we send ASE to a polarizer followed by a PMF section with known length L_0 and then to another polarizer and detect it by an optical spectrum analyzer. From the periodic pattern of the spectrum, the frequency difference $\Delta\omega_0$ between two valleys can be measured. The birefringence Δn is calculated by $\Delta n = 2\pi c/(\Delta\omega_0 L_0)$. We repeated these measurements several times with different lengths of PMD sections, with the result being $\Delta n = 4.15\times 10^{-4}$ within 0.5% error. For the fast axis offset angle θ, when we splice two PMF sections, we set 45° offset on the fiber splicer. We measured several 2-section emulators for which the splicer had been programmed for 45° axis offset and then measured the PSP and DGD spectra experimentally. By fitting our results to Eqs. (3) and (4), we found that the actual splice angle was reproducibly 40° within 0.5° error. Once the systematic error in splicer angle calibration was known, we used this known 40° axis offset angle for our other PMD emulators. As a result, all the estimations show good accuracy. For the 1-section emulator, from Eq. (2) we have 0.2% error to estimate DGD $\Delta\tau$. For the 2-section emulator, from Eq. (3) the estimated DGD $\Delta\tau$ has ~1.5% error, and from Eq. (4) the estimated r has ~1% error. For the 3-section emulator, from Eq. (5) the estimated $\Delta\omega$ has ~0.7% error.

For PMF concatenations of four and more sections, we are not able to accurately predict any parameters of the PMD vector. Thus we validate our measurement results by comparing the results between two different algorithms: the JME and the MMM. Because we use different sets of polarimetery data in these two methods (0°, 90°, and 135° linear polarization states are launched as input SOP for JME, and 0° and RHC are launched for MMM), this procedure is sensitive to the quality of the polarimetry data and is therefore a suitable approach to test the validity of our measurements.

E. Two Different Polarization Mode Dispersion Measurement Methods

The same experimental setup was used to acquire polarimetry data that were analyzed by either the JME [13] or the MMM method [14]. For each case we sequentially cycle through several distinct wavelength-independent launch SOPs into the DUT, in each case recording the output spectral SOP. From the output spectral SOP, we calculate the transmission matrix of DUT, and then the frequency-dependent PMD vectors. Although the JME and MMM techniques are well known, for completeness we introduce them very briefly in the following paragraphs.

In the JME method, the idea is to measure the frequency-dependent Jones matrix of the DUT, from which the PMD vectors can be derived. We launch 0°, 90°, and 135° linear polarization states to DUT. From the three sets of output spectral SOPs, the Jones matrix $T(\omega)$ can be calculated for each frequency. The PMD vector is calculated from eigenanalysis of the matrix $T(\omega+\Delta\omega)T^{-1}(\omega)$. More specifically, the PSPs are the eigenvectors of $T(\omega+\Delta\omega)T^{-1}(\omega)$, and the DGD $\Delta\tau$ is given by [13]

$$\Delta\tau = |\mathrm{Arg}(e_1/e_2)/\Delta\omega|, \tag{6}$$

where e_1 and e_2 are the eigenvalues of $T(\omega+\Delta\omega)T^{-1}(\omega)$. An appropriate size of $\Delta\omega$ is chosen in order to satisfy the condition $\Delta\tau\Delta\omega < \pi$ [13]. Subject to this constraint, a relatively large value of $\Delta\tau\Delta\omega$ (for example, $\Delta\tau\Delta\omega \sim \pi/2$) is desirable in order to reduce the effect of noise.

Similarly, in the MMM method, the PMD vector is extracted from the frequency-dependent Müller matrix. Two different launched SOPs are required. From the two measured output spectral SOPs, the Müller matrix $R(\omega)$ is calculated as a function of frequency. Then the PMD vector is calculated from the matrix $R_\Delta = R(\omega+\Delta\omega)R^T(\omega)$ [14]. More specifically,

$$\cos\phi = (\mathrm{Tr}R_\Delta - 1)/2, \tag{7}$$

$$\begin{aligned} r_1\sin\phi &= (R_{\Delta 23} - R_{\Delta 32})/2, \\ r_2\sin\phi &= (R_{\Delta 31} - R_{\Delta 13})/2, \\ r_3\sin\phi &= (R_{\Delta 12} - R_{\Delta 21})/2. \end{aligned} \tag{8}$$

Here $\mathrm{Tr}R_\Delta$ and $R_{\Delta ij}$ are the trace and the individual elements of the matrix R_Δ respectively, and the PSP is equal to (r_1, r_2, r_3). The DGD is given by

$$\Delta\tau = \phi/\Delta\omega. \tag{9}$$

Similar to the JME, for data processing $\Delta\omega$ should satisfy $\Delta\tau\Delta\omega < \pi$ [14] to avoid issues from higher-order PMD effects. The noise effect is reduced in two ways [14]: choosing a large angle between the two input SOPs (90° on the Poincaré sphere is best, and we use 0° linear and RHC launched SOPs in our experiments) and making $\Delta\tau\Delta\omega$ relatively large, for example $\sim\pi/2$.

In addition to these two methods, the Poincaré arc analysis method [15,16], can also be applied for data obtained with the same experimental setup. The Poincaré arc method calculates the PMD vector from the output SOP spectra directly without first getting the transmission matrix. We have successfully implemented this method as well [17]. However, since the Poincaré arc method has been proved to be equivalent to the JME [18], we do not show the details of this method in this paper.

3. Polarization Mode Dispersion Measurement Results

We now report measurements on several homemade PMD emulators, which are concatenations of several sections of PMF spliced together. In each case the PMD vector is extracted using both JME and MMM algorithms. In addition, DUTs consisting of only one, two, or three sections of PMF are directly compared to accurately estimated parameters.

A. One-Section Emulator

We begin with a single piece of PMF. The fiber length is $L \sim 54$ cm, which gives frequency-independent PMD, with constant DGD ($\sim$0.75 ps) and constant PSP. The output spectral SOP traces out a circle centered at the PSP on the Poincaré sphere. Fig. 4 shows the DGD and PSP data extracted from the frequency-dependent polarimetry data. In Fig. 4(a), the DGDs calculated with JME and MMM methods are very similar. Both versions of the calculated DGD have mean DGD within 0.3% of the expected value and standard deviation (STD) less than 5% of the measured mean DGD. In Fig. 4(b), we show an example of one of the measured output SOP spectra on the Poincaré sphere, for one specific (frequency-independent) input SOP state. We calculate the PMD vector from 3 (2) different such SOP spectra, corresponding to different input SOP states, for analysis by the JME (MMM) method. In particular, although both methods use the same 0° launched polarimetry data, the remaining data sets are distinct: 90° and 135° linear for JME and RHC for MMM. The figure

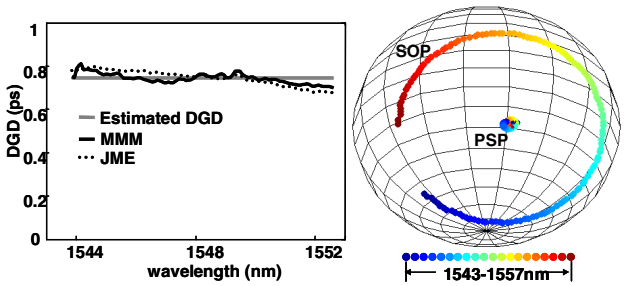

(a) (b)

Fig. 4. (Color online) PMD measurement of 1-section emulator: (a) DGD. The gray line shows the estimated DGD. The black solid line and dashed line show, respectively, DGD calculated by MMM and JME. (b) Output PSP spectra calculated by JME and one output SOP spectra measured.

also shows the frequency-dependent PSP (PSPs for different frequencies are plotted in different colors online) obtained from the JME method. The PSPs calculated from the MMM gave very similar results and are not plotted for the sake of clarity. The PSPs obtained at different frequencies converge almost to a single point, with standard deviation of only 1.4°.

B. Two-Section Emulator

As a slightly more complicated example, we now report measurements for a DUT consisting of two concatenated PMF sections. From the simulation we know that the trajectory of the PSP with frequency is a circle and that the DGD is constant for all frequencies. The DGD and the radius of the PSP circle can be calculated by Eqs. (3) and (4). In this experiment we first performed measurements on a PMD emulator composed of two pieces of PMF with individual lengths of 105 cm and 70 cm and 40° optical axis offset, for which we calculate 1.88 ps DGD. Then we cut back the first fiber in the emulator (from the input side) to obtain a new emulator (70 cm + 70 cm, 40° fast axis offset, for which we calculate 1.48 ps DGD). During the cutback, the second PMF section or the output side SMF lead remains untouched. Figure 5 shows the measurement results. Figure 5(e) gives the DGD (prior to cutback) calculated according to both JME and MMM methods. In both methods the mean DGD has less than 0.6% deviation from the expected value of 1.88 ps; the STD of the calculated DGDs are less than 6% of the measured mean DGD. Figures 5(a)–5(d) show the output SOP spectra for four different launched SOP (0°, 90°, 135°, and RHC, respectively) to illustrate the data from which the PMD vectors are calculated (again before cutback). For the same PMF as Fig. 5(e), i.e., before cutback, the PSP trajectories calculated by the JME and by the MMM are shown in Fig. 5(f) and as the outer circle in Fig. 5(g), respectively. The PSP trajectories on the Poincaré sphere are approximately circles, as predicted. The standard deviation of the data with respect to the best fit circles is 2.7° for JME and 2.1° for MMM. The radii of the best fit circles are both within 5% of the predicted radius. The inner circle in Fig. 5(g) shows the output PSP spectrum after fiber cutback. The PSP trajectories before and after cutback are concentric circles as expected. Furthermore, the PSPs for a specific frequency are oriented similarly on both trajectories. Also as expected, the radius of the trajectory becomes smaller after cutback. Thus, the agreement between experimentally obtained trajectories of the PMD vector and the estimated trajectories based on simple theoretical grounds is excellent.

C. Three-Section and 16-Section Emulators

For concatenation of three pieces of PMF, the DGD is a periodic function of frequency in theory, with period given by Eq. (5). Figure 6(a) shows the DGD of a three-piece PMF (59.3 cm + 118.5 cm + 83 cm, fast axes offset by 45° between the first and the second PMF piece, and by 125° between the second and the third PMF piece; both angles are from the splicer settings). Experimentally, both analysis methods

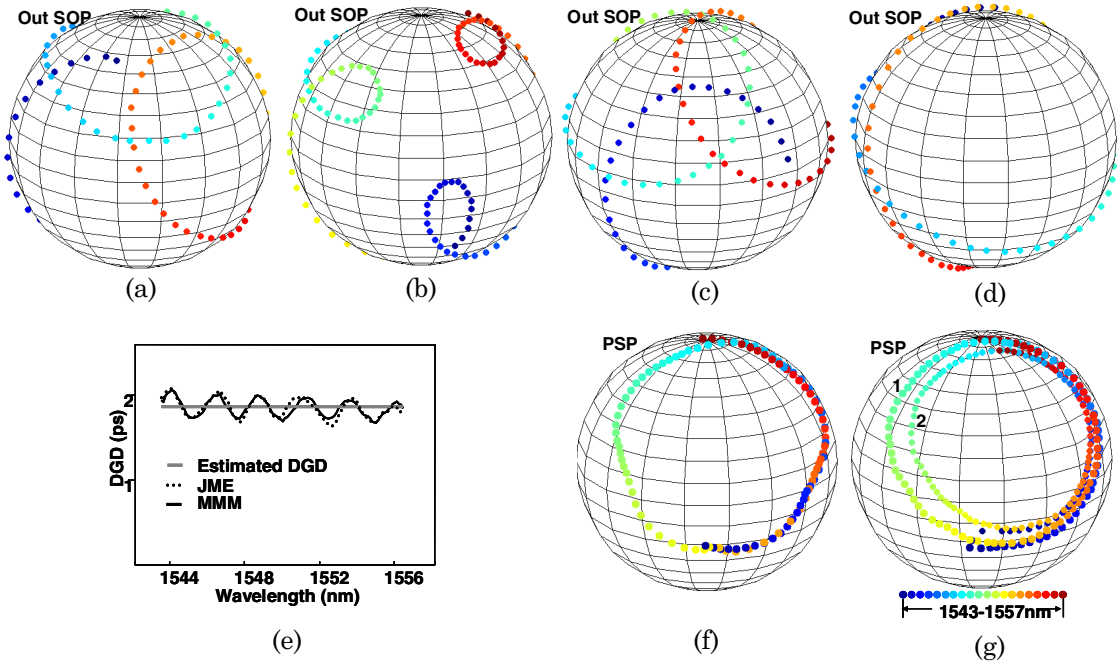

Fig. 5. (Color online) PMD measurement results of 2-section emulators (case 1, 107 cm + 70 cm, 40° fast axis offset, 1.88 ps estimated DGD; case 2, 70 cm + 70 cm, which is obtained by cutting back the input side PMF section of case 1): (a)–(d) four output SOP spectra measured for case 1 corresponding to 0°, 90°, 135°, and RHC launches; (e) DGD of case 1; (f) output PSP spectra of case 1 calculated by JME; (g) output PSP spectra of case 1 and 2 calculated by MMM.

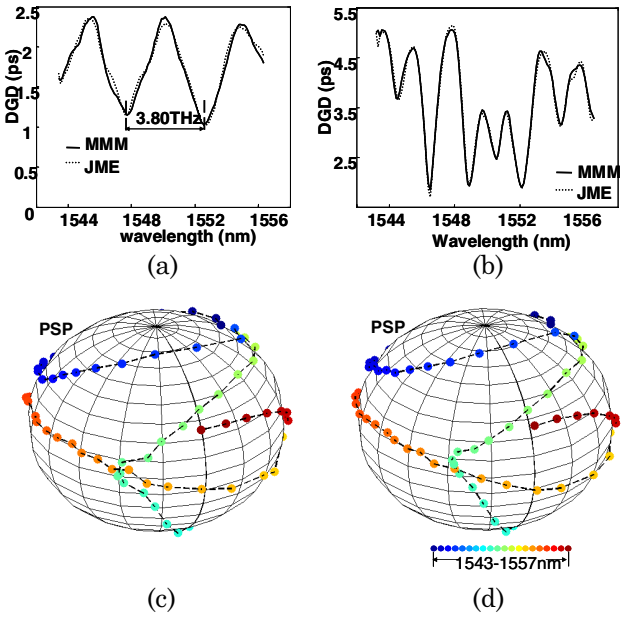

Fig. 6. (Color online) PMD measurement results: (a) DGD for 3-section emulator calculated by MMM and JME. (b)–(d) Results for a 16-section emulator. (b) DGD calculated by JME and MMM. (c) and (d) Frequency-dependent PSP calculated by (c) JME and (d) MMM.

yield similar results for the DGD, in both cases showing periodic behavior with periodicity of approximately 3.80 THz. The experimental periodicity is within 0.8% of the predicted value (3.83 THz).

For the concatenation of more than 3 sections of PMF, there are no predictable parameters against which the experimental results can be directly compared. Nevertheless, we proceeded to construct a 16-section PMF (with total length 465.6 cm), where both the length of each PMF section and the fast axis offset angles between sections were randomly chosen. This results in complicated frequency-dependent PMD, with larger DGD and strong high-order PMD effects. We extract the PMD vector from our measurements using both JME and MMM and compare the results. As shown in Fig. 6(b), the DGDs are very close to each other for these two methods, with 0.08 ps standard deviation and 0.006 ps difference in the mean DGD. Both are small compared to the instantaneous DGD values, which fall in the range 1.9 to 5.2 ps. Figures 6(c) and 6(d), show the PSP evaluated by JME and MMM, respectively. The two trajectories are close to each other with 3.7° mean difference on the Poincaré sphere.

In all these measurements, errors may arise from several factors. First, even for a single frequency, the spot size of light focused onto the camera is larger than one camera pixel; this introduces spectral blurring into the SOP measurements. The impact of the spectral blurring depends both on the PMD of the DUT and on the output SOP. Moreover, other factors such as camera background noise and SOP measurement errors (within 3° on the Poincaré sphere [4]) also introduce error. However, for concatenation of 1 to 3 sections of PMF, the measurement results agree well with simulations and show expected behavior. Moreover, the results from JME and MMM, extracted from different polarimetry data sets, agree closely with each other even for the 16-section emulator with strong high-order PMD. These results confirm that our application of wavelength-parallel spectral polarimetry provides not only high speed but also good accuracy for PMD characterization.

4. Polarization Mode Dispersion Measurement with a Virtually Imaged Phased Array

Based on successful measurements in the above experiment, we modified the setup by using a VIPA [11,12] as the spectra disperser, in order to perform PMD measurement with much higher frequency resolution. The MMM method is adopted here.

A. Measurement Setup

Our experimental setup is shown in Fig. 7(a). A 200 GHz bandwidth (from 1550 nm to 1551.6 nm) of unpolarized light is sliced from an ASE source and amplified by an erbium-doped fiber amplifier. A 4 nm filter is used to suppress noise introduced by the erbium-doped fiber amplifier, and then the light passes through a polarizer. A FLC is used to generate two test SOPs separated by 90° in Stokes space. After transmission through the DUT, optical spectra are dispersed by a VIPA setup in free space and measured by a linear InGaAs camera array with 128 sensing pixels. As a result, the resolution is 1.6 GHz/pixel. For a CW laser beam centered on one camera pixel, the signal detected on the nearest

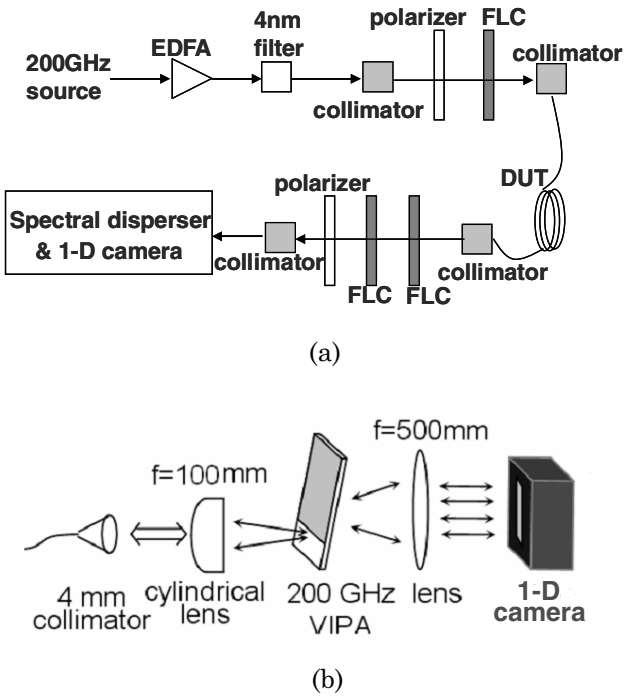

Fig. 7. High spectral resolution measurement setup: (a) full setup and (b) VIPA spectral disperser.

neighbor pixels is suppressed by 6 dB. The details of the VIPA setup are shown in Fig. 7(b). The VIPA setup has 2.5° incident angle and 200 GHz free spectral range. When broadband light is used, frequency components from different free spectral ranges overlap. For this reason we have limited our input spectrum to 200 GHz. The frequencies dispersed by the VIPA are mapped nonlinearly [19] across the camera sensing array. This effect is carefully calibrated and corrected in software subsequent to data acquisition. We use 1-section, 2-section, and 3-section PMFs as the DUTs. In each case we consider short as well as long DUTs. The spliced PMF samples are put in a sealed temperature-controlled box so that the output SOP and the PMD remain stable during the measurement.

B. Measurement Results

1. 1-Section Emulator

The PMD measurement results of a 1-section PMF are shown in Fig. 8. We measured a short piece (12.08 m) of PMF with 16.7 ps estimated DGD and a long one (66.23 m) with 91.6 ps DGD. For the short piece the measured mean DGD is only 1.7% different than the expected value, and the STD is only 1.7% of the measured mean DGD. The PSPs converge to one point with the mean deviation of 2.1° on the Poincaré sphere. For the long piece, the measurement result is also accurate, as shown in Figs. 8(c) and 8(d). The mean DGD is only 0.3% different from the expected value and the STD is only 1.6% of measured mean DGD. The PSPs are close to a single point with standard deviation of only 1.2°. All these measurements show that for 1-section PMF our measurements are accurate for both small and large PMD (~90 ps).

2. 2-Section Emulator

Measurement results of 2-section emulators are shown in Fig. 9. We splice two different 2-section PMFs (8.96 m + 11.04 m and 45.23 m + 21.00 m). In both cases, the angle between fast axes is 40°. Here the DGDs are expected to be 21.3 ps and 73.4 ps, respectively. For the shorter fiber sample, the mean experimental DGD is only 1.0% different from the expected value, and the STD of the DGD measurement is only 2.7% of the measured mean DGD. Moreover the PSP trajectory makes ~2.5 revolutions around a circle as expected (the number of revolutions can be calculated by $\Delta\omega\Delta n L_2/(2\pi c)$), and the radius is within 0.4% of the value predicted by Eq. (4) on the basis of the known splice angle and the relative DGDs of the two fibers. For the long fiber sample the DGD has only 1.3% difference from the expected value, and the STD is only 3.2% of measured mean DGD. The trajectory makes ~5 traces around a circle, and the radius is within 3.6% of the expected value.

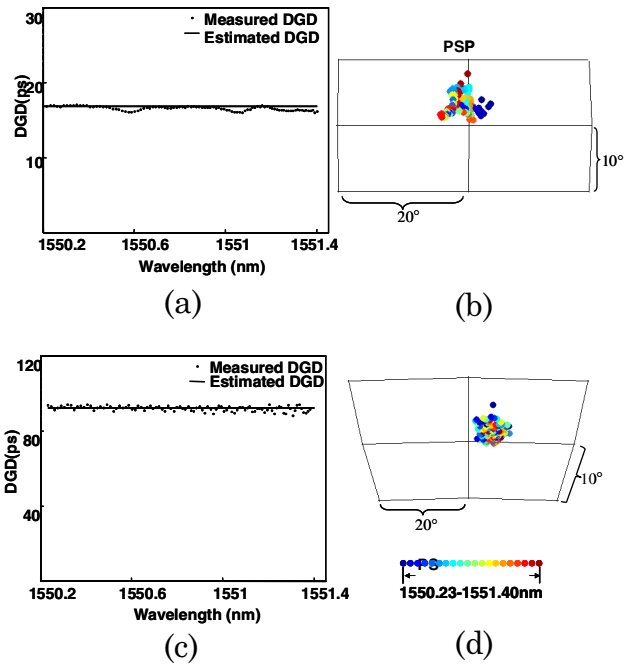

Fig. 8. (Color online) PMD vector measurement results for 1-section emulator: (a) DGD and (b) PSP vector plotted on the Poincaré sphere for a short PMF with estimated 16.7 ps DGD; (c) and (d) DGD and PSP, respectively, for a long PMF with estimated 91.6 ps DGD.

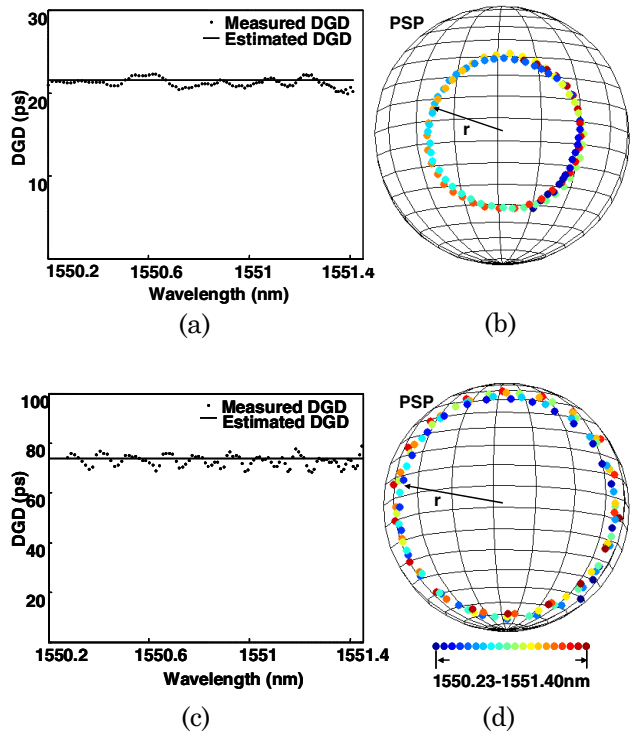

Fig. 9. (Color online) PMD vector measurement results for 2-section emulators: (a) and (b) are DGD and PSP, respectively, for the emulator with estimated 21.3 ps DGD. (c) and (d) are DGD and PSP, respectively, for the emulator with estimated 73.4 ps DGD.

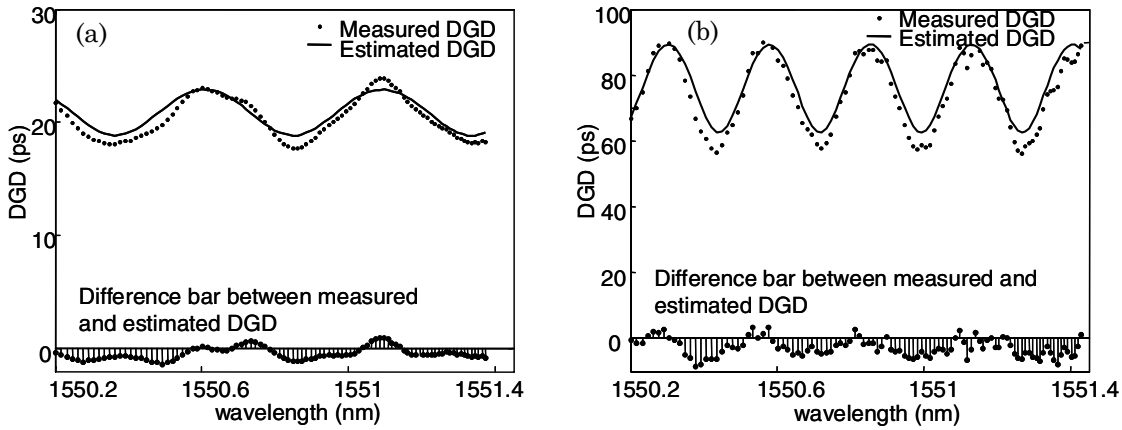

Fig. 10. PMD vector measurement results for 3-section emulators: DGD for (a) short and (b) long emulator.

3. 3-Section Emulator

Measurement results for 3-section emulators are shown in Fig. 10. We spliced together two different 3-section PMFs (4.57 m + 11.91 m + 4.95 m and 45.23 m + 20.95 m + 12.03 m). For each 3-section PMF, the fast axis offset angles at two junctions are both 40°. For concatenations of three pieces of PMF, the frequency-dependent DGD is predicted to be periodic. Though the shape of periodic curve is determined using knowledge of the fiber lengths and splice angles, the start point of the curve (the "phase") is unknown. We tune the start point of the predicted curve to fit the measurement result for comparison. For both the shorter and longer fiber sample, the measured DGD shows good agreement with the predicted curve. The mean difference between measured and predicted DGD spectra is 0.4 ps (1.8% of 22 ps estimated mean DGD) for the shorter emulator and 3.0 ps (3.8% of 77 ps estimated mean DGD) for the longer one.

For the VIPA setup, measurement errors arise from two additional factors. First, since the focused spots at the camera are non-Gaussian in shape, and because spectra map nonlinearly onto the camera sensing array (these effects are inherent to VIPA operation), 60% to 80% of the power of any single frequency falls on its corresponding camera pixel; the remaining power falls on adjacent pixels as crosstalk. Second, inaccuracy in the calibration of the frequency mapping onto the camera pixels can also affect experimental results. Nevertheless, our results show that excellent measurement accuracy is maintained in this high-resolution VIPA-based setup.

5. Conclusion

In summary, we have successfully applied our fast wavelength-parallel spectral polarimetry technology for broadband PMD measurement using both Jones matrix eigenanalysis (JME) and Müller matrix method (MMM) algorithms. We have particularly focused on evaluating the accuracy of our PMD vector measurement results. Our findings indicate that the spectral polarimetry data are of sufficient quality to allow accurate extraction of the PMD spectrum. The spectral polarimetry approach allows fast (potentially on a few milliseconds scale) and efficient measurement of frequency-dependent PMD vectors.

An important point is that the spectral polarimetry approach can be scaled for different optical bandwidths and spectral resolutions via choice of the spectral disperser. Using a grating spectral disperser, we have configured the polarimeter for spectral resolution of ~13.6 GHz/pixel over a 14 nm optical bandwidth. By using a VIPA spectral disperser, a higher resolution (1.6 GHz/pixel) is obtained over a 200 GHz band. This has potential to be used for PMD sensing in optical fiber communication systems at 40 Gbit/s and beyond. In the future, by using a two-dimensional VIPA-grating spectral disperser [12], fast PMD measurement of over 1000 frequency samples spanning essentially the full C band should be possible.

We are grateful to Daniel E. Leaird and Peter J. Miller for valuable discussions and comments. This work was funded by the National Science Foundation (NSF) under grant ECS-0501366.

References

1. H. Kogelnik, R. M. Jopson, and L. E. Nelson, "Polarization mode dispersion," in *Optical Fiber Telecommunications IVB–Systems and Impairments*, I. P. Kaminow and T. Li, ed. (Academic, 2002), Chap. 15, pp. 725–863.
2. M. Karlsson, J. Brentel, and P. A. Andrekson, "Long-term measurement of PMD and polarization drift in installed fibers," J. Lightwave Technol. **18**, 941–951 (2000).
3. H. Bülow, "Limitation of optical first-order PMD compensation," in *Optical Fiber Communication Conference 1999/International Conference Integrated Optics and Optical Fiber Communication (OFC/IOOC '99) Technical Digest* (Optical Society of America, 1999), Vol. 2, pp. 74–76.
4. S. X. Wang and A. M. Weiner, "Fast wavelength-parallel polarimeter for broadband optical networks," Opt. Lett. **29**,923–925 (2004).
5. S. X. Wang and A. M. Weiner, "A complete spectral polarimeter design for lightwave communication systems," J. Lightwave Technol. **24**, 3982–3991 (2006).
6. S. X. Wang, A. M. Weiner, S.-H. Foo, D. Bownass, M. Moyer, M. O'Sullivan, M. Birk, and M. Boroditsky, "PMD tolerance

testing of a commercial communication system using a spectral polarimeter," J. Lightwave Technol. **24**, 4120–4126 (2006).
7. M. Boroditsky, K. Cornick, C. Antonelli, M. Brodsky, S. D. Dods, N. J. Frigo, and P. Magill, "Comparison of system penalties from first and multi-order PMD," IEEE Photon. Technol. Lett. **17**, 1650–1652 (2005).
8. M. Akbulut, A. M. Weiner, and P. J. Miller, "Wideband all-order polarization mode dispersion compensation via pulse shaping," Opt. Lett. **30**, 2691–2693 (2005).
9. H. Miao, A. M. Weiner, L. Mirkin, and P. J. Miller, "All-order polarization mode dispersion compensation (PMD) via virtually imaged phased-array (vipa) based pulse shaper," IEEE Photon. Technol. Lett. **20**, 545–547 (2008).
10. L. Xu, H. Miao, and A. M. Weiner, "Fast measurement of polarization mode dispersion via virtually imaged phased-array based spectral polarimetry," presented at the Optical Fiber Communications Conference, San Diego, California, 24–29 February, 2008.
11. M. Shirasaki, "Large angular dispersion by a virtually imaged phased array and its application to a wavelength demultiplexer," Opt. Lett. **21**, 366–368 (1996).
12. S. X. Wang, S. Xiao, and A. M. Weiner, "Broadband, high spectral resolution 2-D wavelength-parallel polarimeter for dense WDM systems," Opt. Express **13**, 9374–9380 (2005).
13. B. L. Heffner, "Automated measurement of polarization mode dispersion using Jones matrix eigenanalysis," IEEE Photon. Technol. Lett. **4**, 1066–1069 (1992).
14. R. M. Jopson, L. E. Nelson, and H. Kogelnik, "Measurement of second-order polarization-mode dispersion vectros in opitcal fibers," IEEE Photon. Technol. Lett. **11**, 1153–1155 (1999).
15. C. D. Poole, Neal. S. Bergano, R. E. Wagner, and H. J. Schulte, "Polarization dispersion and principal states in a 147 km undersea lightwave cable," J. Lightwave Technol. **6**, 1185–1190 (1988).
16. P. B. Phua and H. A. Haus, "All-frequency PMD compensator in feedforward scheme," J. Lightwave Technol. **22**, 1280–1289 (2004).
17. L. Xu, S. X. Wang, and A. M. Weiner, "Broadband polarization mode dispersion measurement via spectral polarimetry," presented at Frontiers in Optics 2006, Rochester, New York, 8–12 October 2006.
18. N. Cyr, "Equivalence of Poincaré sphere and Jones matrix analyses for determination of PMD," presented at the OFMC '99 convention, Nantes, France, 1999.
19. S. Xiao, A. M. Weiner, and C. Lin, "A dispersion law for virtually imaged phased-array spectral dispersers based on paraxial wave theory," IEEE J. Quantum Electron. **40**, 420–426 (2004).